OIL SPILL DETECTION IN ENVISAT ASAR IMAGES USING RADAR BACKSCATTER THRESHOLDING AND LOGISTIC REGRESSION ANALYSIS

Jojene R. Santillan*[1] and Enrico C. Paringit[2]

[1]University Research Associate, Applied Geodesy and Space Technology Research Laboratory, Training Center for Applied Geodesy and Photogrammetry, Osmeña Avenue, University of the Philippines, Diliman, Quezon City 1101, Philippines; Tel: +63-2-9818500#3147; Email: jrsantillan@up.edu.ph

[2]Associate Professor, Department of Geodetic Engineering, College of Engineering, Osmeña Avenue, University of the Philippines, Diliman, Quezon City 1101, Philippines; Tel: +63-2-9208924; E-mail: ecparingit@up.edu.ph

KEY WORDS: Oil spill detection, radar backscatter thresholding, logistic regression, Envisat ASAR, MT-Solar oil spill, Guimaras, Philippines

ABSTRACT: This paper presents a technique to detect oil spills in ENVISAT Advanced Synthetic Aperture Radar (ASAR) images using radar backscatter thresholding and logistic regression analysis. We developed and tested this technique using 4 Envisat ASAR images that were acquired many days after the M/T Solar I oil spill incident occurred on August 11, 2006 in Panay Gulf, southwest of Guimaras Island in Visayas, Philippines. A semi-automated approach by histogram analysis and radar backscatter thresholding was implemented to detect and segment dark formations in the Envisat ASAR images. Then, a logistic regression (LR)-based dark formation classifier was developed using 4 shape features, 11 contrast features, 2 homogeneity, and 2 slick surrounding features of the detected dark formations consisting of 154 verified oil slicks and 1,355 look-alikes. From this, a dataset consisting of 77 confirmed oil slicks and 77 look-alikes were randomly selected and used to train the classifier while the remaining dataset of 77 oil slicks and 1,272 look-alikes were used for validation. Features of the training dataset were fitted in a binary LR model and a backward stepwise-likelihood ratio approach was utilized to determine the sets of features that best discriminate an oil slick from its look-alike. Cross-validation of the LR classifier using the training dataset showed 84% accuracy for oil slick classification, 87% accuracy for look-alike classification, and an overall classification accuracy of 86%. An independent validation of the LR classifier revealed an above average performance, with 92% accuracy for oil slick classification, 76% accuracy for look-alike classification, and overall classification accuracy of 77%. The results of this study indicate that the combined radar backscatter thresholding and logistic regression analysis could be a promising approach in oil spill detection in Envisat ASAR images. The simplicity of the technique and its use of information readily available from the SAR images are advantageous in the rapid mapping of oil slicks right after an oil spill incident. Its improvement through consideration of prevailing wind conditions, the use of large training and validation datasets as well as inclusion of other relevant image features during classifier development could be a subject of future studies.

1. INTRODUCTION

1.1 Background and motivations

Images acquired by spaceborne Synthetic Aperture Radar (SAR) sensors have been extensively used for the detection of oil spills in the marine environment (Brekke and Solberg, 2005a; Topouzelis, 2008). Oil spill detection from SAR images relies on the fact that oil film decreases the backscattering of the sea surface resulting in dark formation that contrasts with the brightness of the surrounding spill-free sea. In a recent review by Topouzelis (2008), several semiautomatic and fully automatic methodologies have been developed for oil spill detection in SAR images. However, they are not very popular for oil spill detection as they are complex, they can not be easily reproduced and require specific knowledge on image understanding, pattern recognition and classifications theories.

In the vast literature of oil spill detection from SAR images, the logistic regression (LR) approach has not been used yet as a dark formation classifier though many statistical-based approaches have been reported (Topouzelis, 2008). LR's potential as a binary classifier have been maximized in medical imaging applications (Ayer et al., 2010; Dreiseitl and Ohno-Machado, 2002) such as in classifying pigmented skin lesions (Dreiseitl et al., 2001), in computer-aided detection and diagnosis of benign and malignant breast masses in ultrasound images (Song et al., 2005) and prediction of malignant breast lesions on dynamic contrast-enhanced magnetic resonance images (McLaren et al., 2009). In these applications, LR is used to examine the relationship between a binary outcome (dependent) variable such as presence or absence of disease and predictor (explanatory or independent) variables such as image features and/or patient demographics. In Dreiseitl et al. (2001), the discriminatory power of LR and other

machine learning algorithms such as k-nearest neighbor, artificial neural network (ANN), decision trees and support vector machines were analyzed on the task of classifying images of pigmented skin lesions. The algorithms were trained and tested on a dataset of morphometric features of pigmented skin lesions extracted from the images that were categorized into global (shape, color, normalized color, border features) and local (segment, quantized color, ratio) features. Of the five methods investigated, excellent classification results were obtained for logistic regression, with its performance almost identical to those of artificial neural networks and support vector machines. In Song et al. (2005), ultrasound images of 24 malignant and 30 benign masses were analyzed quantitatively for margin sharpness, margin echogenicity, and angular variation in margin. These features and age of patients were used with two pattern classifiers, LR and ANN, to differentiate between malignant and benign masses. The performance of two methods was compared by Receiver Operating Characteristics (ROC) analysis. Results of this study showed that there was no difference in performance between LR and the ANN as measured by the area under the ROC curve. However, logistic regression analysis is more advantageous because it provides a deterministic model for the data and yields weighting factors for each contributing feature. The LR classifier was also less complex to develop and faster to train than ANN. In McLaren et al. (2009), a logistic regression-based computer aided diagnosis system was trained to automatically analyze breast lesion features detected from magnetic resonance images in order to differentiate between malignant and benign lesions. For the selection of the best predictors of malignant lesions, the LR-classifier utilized eight morphologic parameters, 10 gray-level co-occurrence matrix texture features, and 14 Laws texture features that were obtained using automated lesion segmentation and quantitative feature extraction.

It is clear from the literatures cited above that although medical imaging is an entirely different field from SAR remote sensing, the principle, approach and procedures in object detection and classification from the images are just the same. The only difference, however, is the type of image being analyzed and the object to detect and classify. Moreover, medical applications of LR approach as a classifier are based on inherent image features of objects as indicators of whether it belongs to a certain class or otherwise. In oil spill detection, specifically in dark formation classification, the use of object features as input to a classifier is of similar importance. In this context, the LR approach can be an effective classifier of oil spills and look-alikes.

1.2 Objectives

The goal of this paper is to present an uncomplicated approach in dark formation detection and oil spill classification from Envisat Advanced SAR images through radar backscatter thresholding and application of logistic regression analysis. The technique is envisioned to be an alternative to existing statistically-based oil spill detection and classification approaches.

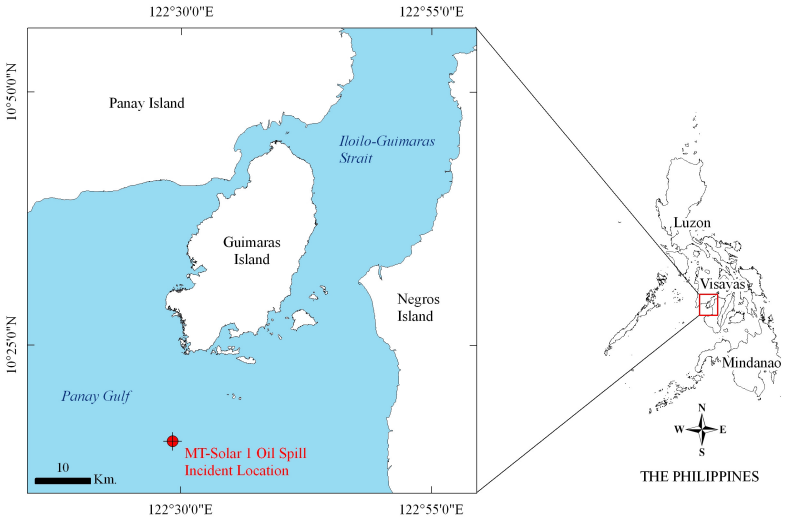

Figure 1. Map showing the location of the August 11, 2006 MT-Solar 1 oil spill incident near Guimaras Island, Visayas, Philippines.

2. METHODS

The oil spill detection technique to be presented in this paper follows the three steps generally employed in SAR-based oil spill detection (Topouzelis, 2008): (i.) detection and isolation of all dark formations in the image, (ii.) extraction of statistical parameters of the dark formations ("features") that are related to the geometry of the formation, physical behavior, and their context on the image, and (iii.) classification of the dark formations to oil spills or look-alikes. We developed and tested this technique using Envisat Advanced Synthetic Aperture Radar (ASAR) images of the August 11, 2006 MT-Solar 1 oil spill incident that occurred in Panay Gulf, southwest of Guimaras Island in Visayas, Philippines (Figure 1). This oil spill event is considered to be the worst oil-related environment disaster the Philippines has experienced.

2.1 Envisat ASAR Images of the August 11, 2006 MT-Solar 1 Oil Spill

Four (4) Level 1P (slant- and ground-range corrected) Envisat ASAR images of the MT-Solar 1 oil spill were provided by the European Space Agency (ESA) through a Category 1 (Cat-1) project. These images were acquired in

Wide Swath Mode (WSM) and provided by ESA as amplitude images with pixel width of 75 m. The dates and times of acquisition are as follows: (1) 24 August 2006, 1:44:41 UTC; (2) 25 August 2006, 13:53:16 UTC; (3) 28 August 2006, 13:55:58 UTC; and (4) 06 September 2006, 1:36:09 UTC. Standard radar image pre-processing procedures using ESA's Basic ENVISAT SAR Toolbox (BEST) version 4.2.2 software were applied to the Envisat ASAR amplitude images. This included radiometric calibration to generate a backscatter (β) image, and geometric correction to georeference the input ASAR images into the Universal Transverse Mercator Zone 51 projection with the World Geodetic System 1984 as datum. The images were then exported to Environment for Visualizing Images (ENVI) software version 4.3 for further analysis. Here, the images were "de-speckled" using a 3x3 Enhanced Lee filter. This removed the noisy pixels in the images while preserving texture information. Finally, land masses were masked out from the images using a vector database of island boundaries digitized from 1:50,000 topographic maps of the same area.

2.2 Dark Formation Detection

Dark spots/formations detection and segmentation from the pre-processed Envisat ASAR images were implemented in a semi-automated approach by histogram analysis and radar backscatter thresholding. The main goal is to detect all suspicious slicks and to preserve the slick shapes. The latter is of most importance for the success of discriminating oil spills from look-alikes (Brekke and Solberg, 2005a). To allow a consistent use of thresholding factor for dark formation detection, normalization was done in such a way that the minimum and maximum β values of sea surface in all the images are the same. The 24 August 2006 image was used as reference, and all the other three images were normalized to this image. After normalization, basic statistics of the sea surface β values in each image were computed (minimum, maximum, mean and standard deviation, σ). Histogram of β values were likewise plotted and analyzed. Image visualizations indicate that dark formations have the smallest β values, ranging from β_{min} to a certain threshold. The value of this threshold was obtained experimentally by using the β_{mean} as a starting level. Several image thresholding factors that were used to detect dark spots/formations through "density slicing" in ENVI 4.3 included β_{mean}, $\beta_{mean} - 0.5\sigma$, $\beta_{mean} - 0.75\sigma$, $\beta_{mean} - \sigma$ and $\beta_{mean} - 2\sigma$. The best result (over 4 images) was found using the $\beta_{mean} - 0.75\sigma$ threshold; hence, all pixels equal or below this value were considered as dark spot or part of a dark formation. The dark spots/formations detected were then subjected to segmentation to derive regions of connected pixels. ENVI 4.3's segmentation algorithm based on connectivity of a pixel was used. The algorithm works by analyzing each dark spot pixel and its neighbors. If a pixel is connected to a least 4 neighbors, then they will form a segment. The analysis was able to detect and isolate 1,509 dark formations from the 4 Envisat ASAR images (594 for August 24, 192 for August 25, 337 for August 28, and 386 for September 6). A manual analysis of the slicks was done prior to this to classify which of the slicks are oil spills and which ones are look-alikes. Oil spill maps published by UNOSAT (2006) and World Wildlife Fund-Philippines (Ligtas Guimaras, 2006), and field reports by the Silliman University Marine Laboratory (2006) were used as references in this manual classification. This resulted to 154 oil slicks and 1,355 look-alikes.

2.3 Feature Extraction

The segmented dark spots/formations, hereafter referred to as "slicks", were then exported to vector format and further manipulated in Arcview GIS ver. 3.2 software. For each slick, a set of features were computed. These features were later used to classify each slick as either oil or look-alike. The feature set consists of a mix of features that have been used for oil spill detection as well as traditional descriptors from the image analysis literature (Brekke and Solberg, 2005b; Stathakis et al., 2006; Solberg et al., 2007; Topouzelis, 2008). These features (total of 17), grouped into descriptors for shape, contrast, slick homogeneity and slick surroundings are listed in Table 1. The *dist2riv* feature was included in this study as it was hypothesized that the high discharge rate from the rivers may have affected the movement of oil slicks, dispersing them away from the coastal areas where major rivers are located. This is also in consideration of the stormy weather conditions prevalent during the oil spill event that may have generated huge runoff volume being drained to the sea. The "larger window" surrounding the slick region that is used for computing background-related contrast features has no definite length and width (or diameter) and could be adaptive depending on the horizontal and vertical extent of a slick. In this study, a circular window is used, with its center at the midpoint of the line connecting the extreme points of the slick region and with diameter equal to the Euclidean distance between the two extreme points.

Table 1. Features computed for all the detected candidate slicks.

Feature	*Description*
Shape features (4)	
a. Slick area, A	The area of the slick region, in km^2.
b. Slick perimeter, P	Perimeter of the slick region, in km.
c. Slick complexity, C	$C = P^2/A$

(continuation of Table 1)

d. Slick perimeter to area ratio	*P/A*
Contrast features (9)	
a. Slick mean backscatter value, μ_{slick}	Mean of slick backscatter values.
b. Slick standard deviation, σ_{slick}	Standard deviation of slick backscatter values.
c. Slick minimum backscatter value, min_{slick}	Minimum of slick backscatter values.
d. Slick maximum backscatter value, max_{slick}	Maximum of slick backscatter values.
e. Background mean backscatter value, μ_{bkgrd}	Mean backscatter value of slick background within a larger window surrounding the slick.
f. Background standard deviation, σ_{bkgrd}	Standard deviation of backscatter values of slick background within a larger window surrounding the slick.
g. Background minimum backscatter value, min_{bkgrd}	Minimum of backscatter values of slick background within a larger window surrounding the slick.
h. Background maximum backscatter value, max_{bkgrd}	Maximum of backscatter values of slick background within a larger window surrounding the slick.
i. Slick local contrast, *SLC*	The difference between the mean backscatter value of the slick and the mean backscatter value of slick background within a larger window surrounding the slick
Homogeneity (2)	
a. Slick power-to-mean ratio, PMR_{slick}	$\sigma_{slick}/\mu_{slick}$
b. Background PMR, PMR_{bkdrg}	$\sigma_{bkgrd}/\mu_{bkgrd}$
Slick surroundings (2)	
a. Distance to sunken vessel location, *dist2ship*	The Euclidean distance of the center of the slick region to the sunken vessel location, in km.
b. Distance to mouth of rivers, *dist2riv*	The Euclidean distance of the center of the slick region to the nearest mouth of rivers, in km.

2.4 LR-based Classifier Development

Theoretical Background of LR Analysis: Logistic regression (Hosmer and Lemeshow, 2000) is a simple and efficient supervised classification method that provides explicit probabilities of class membership and an easy interpretation of the regression coefficients of predictor variables. It is commonly used to analyze dichotomous outcomes (dependent variable) and is particularly appropriate for models involving decision-making. The dichotomous dependent variable is usually coded as 0 or 1 while the independent variables may be continuous, categorical, or a combination of the two, and does not require strong assumptions, like gaussianity of the predictor variables given the class or assumptions about the correlation structure (Bielza et al., 2011).

The concept behind logistic regression as a classifier can be extended into the oil spill detection problem. In oil spill detection, a dichotomous outcome of interest is whether a dark formation detected in a SAR image is an oil spill or a lookalike: *Y=1* if it is an oil spill or *Y=0* if it is a lookalike. In the logistic model, the expected value of the response *Y* is equal to the probability that *Y =1*, that is, the probability that an event (such an oil spill) is present in the image. If $X_1, X_2, \ldots, X_n$ denote *n* predictor variables (e.g., shape, contrast, slick homogeneity and slick surroundings features), and *p* denotes the probability of oil spill presence in the image (i.e., the probability that $Y = 1$), the relationship between the predictor variables and *p* can be expressed as $Log\left(\frac{p}{1-p}\right) = B_0 + B_1X_1 + \ldots + B_nX_n$, or equivalently as $p(Y=1) = \frac{e^{B_0+B_1X_1+\ldots+B_nX_n}}{1+e^{B_0+B_1X_1+\ldots+B_nX_n}}$, where B_0 is a constant and $B_1, B_2, \ldots, B_n$ are the regression coefficients of the predictor variables $X_1, X_2, \ldots, X_n$. Each regression coefficient, estimated from the available data, describes the size of the contribution of the corresponding predictor variable to the outcome. The probability of oil spill presence *p* can then be estimated with this equation. A common cut point for classifying cases is p=0.5; *p* values computed for each candidate slick that exceed the classification cutoff are classified as oil, while those with predicted values smaller than the cutoff are classified as lookalike.

Developing the LR-based Oil Spill Classifier: The LR-based classifier was developed using the 4 shape features, 9 contrast features, 2 homogeneity and 2 surrounding features of the detected slicks in the 4 Envisat ASAR images (Table 2). SPSS version 16 was used in training the logistic regression classifier, wherein features of 77 oil slicks and 77 look-alikes (i.e., the training dataset randomly selected from the 4 images) were fitted in the LR equation. A balanced dataset of oil and lookalike was used in classifier training to avoid erroneous fit of the model, which is likely

to happen when the ratio 0/1 observations for the response variable is out of proportion, meaning an excess of 0's compared to 1's or the other way around (Van Doorn and Bakker, 2007). A backward stepwise-likelihood ratio approach was used to determine the sets of features (X_i) with the largest significance in the classification model (i.e., the features that best discriminate an oil slick from its look-alike), their corresponding coefficients (B_i) and the model constant B_0. A backward stepwise-likelihood ratio approach works by including all the predictor variables in the model and the variables are removed one by one as they are found to be insignificant in predicting the outcome (Ayer et al., 2010). Performing variable selection is a way to reduce a model's complexity and consequently decrease the risk of overfitting (Dreiseitl and Ohno-Machado, 2002). The LR-based classifier was validated with the remaining dataset of 77 oil spills and 1,278 lookalikes.

Table 2. Oil spill and lookalike datasets used for training and testing the LR-based classifier. The slicks for training and testing were selected using proportionate random sampling from each image.

Envisat ASAR Image	*Total Number of Slicks*		*Training Dataset Only*		*Testing Dataset Only*	
	Lookalike	*Oil*	*Lookalike*	*Oil*	*Lookalike*	*Oil*
Aug. 24, 2006	567	27	14	14	553	13
Aug. 25, 2006	156	36	18	18	138	18
Aug. 28, 2006	291	46	23	23	268	23
Sept. 06, 2006	341	45	22	22	319	23
Total	1,355	154	77	77	1,278	77

3. RESULTS AND DISCUSSIONS

3.1 The LR-based Oil Spill Classifier

Equation (1) below summarizes the LR-based oil spill classifier containing the significant features (X_i) that best discriminate an oil slick from its look-alike in Envisat ASAR images, their corresponding coefficients (B_i) and the model constant B_0. Among the 17 features used, only 9 were found to be the most significant in classifying oil slicks and look-alikes. Three of these are contrast features such as slick background standard deviation (σ_{bkgrd}), slick background mean (μ_{bkgrd}), and slick mean (μ_{slick}). The rests are related to homogeneity (PMR_{bkdrg}), slick shape (A, P) and slick surroundings (*dist2ship*, *dist2riv*).

$$P(Y=1) = \frac{e^z}{1+e^z}$$

$$where\ z = -56.377 - 72.957\sigma_{bkdrg} + 42.954PMR_{bkdrg} + 3.292\mu_{bkdrg} - 2.311\mu_{slick} - 0.350A - 0.152dist2ship - 0.141dist2riv + 0.074P \quad (1)$$

It can be observed from the B_i values that among the 9 significant features, PMR_{bkdrg} and σ_{bkgrd} have the highest contribution in terms of increasing or decreasing the probability of a candidate slick being an oil spill. It is clear from the B_i values that slick background features are relevant features in oil spill classification. The positive regression coefficients of PMR_{bkdrg}, μ_{bkgrd}, and P indicate that these features increases the probability of a candidate slick being classified as an oil spill. On the other hand, the probability of oil spill detection is decreased by σ_{bkgrd}, μ_{slick}, A, *dist2ship* and *dist2riv*. The B_i values can be interpreted further when classifying two or more candidate slicks. According to the signs of the coefficients, it can be inferred that a slick with high values of PMR_{bkdr}, μ_{bkgrd} and P but with small values of σ_{bkgrd}, μ_{slick}, A, *dist2ship* and *dist2riv* will have a probability of being an oil spill. The reverse of this would indicate that the slick could be a lookalike. The LR equation also implies that candidate slicks farther from the spill source and from rivers (high *dist2ship* and *dist2riv* values) have low probabilities of being oil spills. It is clear from the LR equation that although *dist2ship*, *dist2riv*, A and P are significant predictors of oil spill, their respective contribution is lower compared to σ_{bkgrd}, PMR_{bkdrg} ,μ_{bkgrd}, and μ_{slick}. The large and negative value of the equation constant (B_0) could be an indicator that other features (apart from the 17 features) may have been omitted in this study, especially during classifier training. These features may be related to textural information such as slick border gradients, slick curvature, etc. (Solberg et al., 2007). Further studies are necessary to evaluate the contribution of the omitted features.

3.2 Accuracy of the LR-based Oil Spill Classifier

Table 3 shows the results of the LR-based classifier as applied to the training (cross-validation) and test (validation) datasets. In cross-validation, the LR classifier's performance was satisfactory, correctly classifying 84% of the oil slicks (65 of 77), and 87% of the lookalikes (67 of 77). For this dataset, the overall classification accuracy was at 86%. In the independent validation using the test dataset, the LR classifier's performance was found to be generally acceptable, with an overall classification accuracy of 77%. For this dataset, the oil spill classification was very high at

92% (71 of 77) while lookalike classification was found reasonable at 76% (968 of 1278). It can be observed that the classifier is very good in classifying oil spills. However, it appears to perform low in classifying lookalikes, misclassifying 310 lookalikes as oil spills. Nevertheless, the classifier's performance is promising in oil spill and lookalike classifications.

Table 3. Confusion matrix showing the results of logistic regression classification as applied to the training and test datasets.

Training Dataset (Cross-validation)		*Classification*			% Correct
		Lookalike	Oil	Total	
Sea-truth	Lookalike	**67**	10	77	87
	Oil	12	**65**	77	84
	Total	79	75	**132**	86

Test Dataset (Validation)	*Classification*			% Correct
	Lookalike	Oil	Total	
Lookalike	**968**	310	1,278	76
Oil	6	**71**	77	92
Total	974	381	**1,039**	77

To visualize the results of the classification, the LR-based classifier was applied to each of the 4 Envisat ASAR images. The classified images are shown in Figure 2 while the percentage accuracies are listed in Table 4. It can be observed that the LR-based classifier has satisfactory performance in classifying oil spills and lookalikes. For all the images, the overall classification accuracy is greater than 70%. However, the classifier has difficulty in correctly classifying the lookalikes.

Table 4. Accuracies of the LR-based classifier as applied to the 4 Envisat ASAR images.

Envisat ASAR Image	*Overall Classification Accuracy (%)*	*Oil Spill Classification Accuracy (%)*	*Lookalike Classification Accuracy (%)*
Aug. 24, 2006	78	67	78
Aug. 25, 2006	72	94	67
Aug. 28, 2006	74	98	71
Sept. 06, 2006	83	87	83

4. CONCLUSIONS AND RECOMMENDATIONS

In this paper, a technique to detect oil spills in Envisat ASAR images using radar backscatter thresholding and logistic regression analysis was presented. The technique consist of three major steps: (i.) dark formation detection through image normalization, histogram analysis and backscatter thresholding, (ii.) feature extraction, and (iii.) oil spill classification using LR analysis. The results of this study showed that the combined radar backscatter thresholding and LR-based classifier could be a promising approach in oil spill detection in Envisat ASAR images. An added value explored in this study is its findings on the relative contribution of image features in the detection and discrimination of oil spills from look alike. The analysis revealed that slick background features PMR_{bkdrg} and σ_{bkgrd} have the highest contributions in increasing and decreasing, respectively, the probability of candidate slicks detected in the Envisat ASAR images as being oil spills. The simplicity of the technique and its use of information readily available from the SAR images are advantageous in the rapid mapping of oil slicks right after an oil spill incident. The LR-based classifier can also be of great value when doing historical mapping of oil spills such as finding where the oil spills have been (their relative movements through time and space), and the location of coastal areas affected. This is useful for studies that require information for the assessment of the damages of oil spills in the coastal environment.

While the technique showed satisfactory results, its improvement through consideration of prevailing wind conditions, the use of large training and testing datasets as well as inclusion of other relevant image features during classifier development could be a subject of future studies. It is emphasized here that the LR-based oil spill classifier was developed using oil slick and lookalike datasets that were pre-classified using secondary information from published oil spill maps. Confidence in the classification results can be enhanced if the classifier is to be developed and tested on a SAR dataset of oil spills and lookalikes that were actually verified through site inspection. Testing the classifier in an image without oil spills as well as comparing its performance with other classifiers are also worth doing as these could help further determine the accuracy of the classifier.

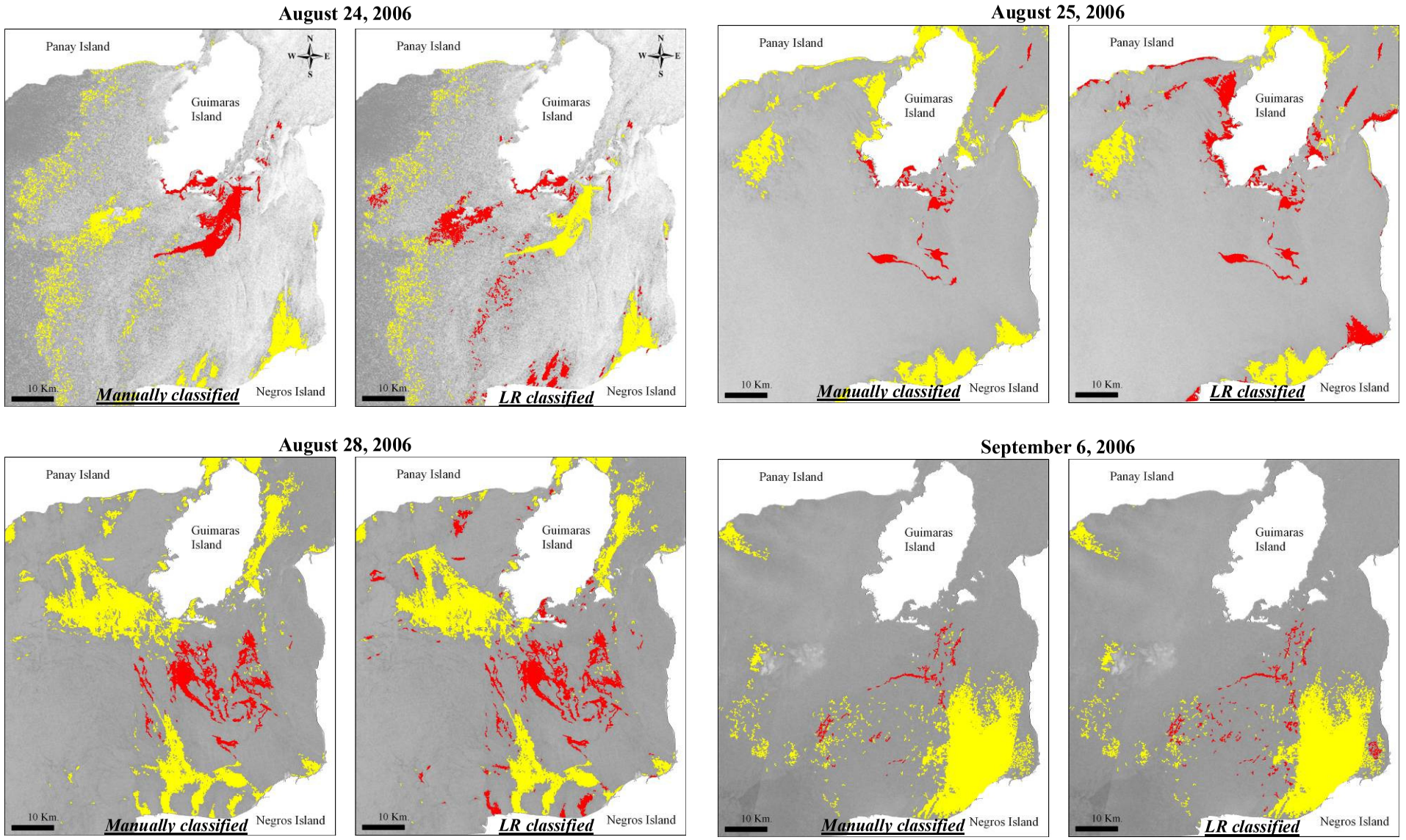

Figure 2. Oil spills and lookalikes detected in 4 Envisat ASAR images using manual classification and using the LR-based oil spill classifier. Legend: oil spill, lookalike. Envisat ASAR Images © European Space Agency (2006).

ACKNOWLEDGEMENTS

The Envisat ASAR images were generously provided by the European Space Agency (ESA). This work was part of a Grant-In-Aid project, "Development of Geospatial Techniques to Analyze Impacts of Oil Spills on Coastal Resource and Environment", funded by the Philippine Council for Advanced Science and Technology Research and Development (PCASTRD) of the Department of Science and Technology (DOST).

REFERENCES

Ayer, T., Chhatwal, J., Alagoz, O., Kahn, C., Woods, R., Burnside, E., 2010. Informatics in radiology: comparison of logistic regression and artificial neural network models in breast cancer risk estimation. Radiographics, 30, pp. 13-22.

Bielza, C., Robles, V., Larrañaga, P., 2011. Regularized logistic regression without a penalty term: an application to cancer classification with microarray data. Expert Systems with Applications, 38, pp. 5110-5118.

Brekke, C., Solberg, A., 2005a. Oil spill detection by satellite remote sensing. Remote Sensing of Environment, 95(1), pp. 1–13.

Brekke, C., Solberg, A., 2005b. Feature extraction for oil spill detection based on SAR images. In: Image Analysis, Lecture Notes in Computer Science, edited by Kalviainen, H., Parkkinen, J., and Kaarna, A., Vol. 3540. Springer Berlin / Heidelberg, pp. 111-125.

Dreiseitl, S., Ohno-Machado, L., 2002. Logistic regression and artificial neural network classification models: a methodology review. Journal of Biomedical Informatics, 35(5-6), pp. 352-359.

Dreiseitl, S., Ohno-Machado, L., Kittler, H., Vinterbo, S., Billhardt, H., Binder, M., 2001. A comparison of machine learning methods for the diagnosis of pigmented skin lesions. Journal of Biomedical Informatics, 34(1), pp. 28–36.

Hosmer, D. W., Lemeshow, S., 2000). Applied Logistic Regression (2nd ed.). John Wiley & Sons, New York, USA.

Ligtas Guimaras, 2006. Satellite images and maps of the MT-Solar 1 oil spill. Retrieved from http://www.ligtasguimaras.com.ph/satelliteimages.asp

McLaren, C. E., Chen, W.P., Nie, K., Su, M.Y. 2009. Prediction of malignant breast lesions from MRI features: a comparison of artificial neural network and logistic regression techniques. Academic Radiology, 16(7), pp. 842-851.

Silliman University Marine Laboratory. (2006). Final Report: M/V Solar 1 Oil Spill Rapid Assessment, August 25-30, 2006. Retrieved April 27, 2008, from http://web.kssp.upd.edu.ph/oil_spills/oil%20spills%20fora.html

Solberg, A., Brekke, C., Husoy, P., 2007. Oil spill detection in Radarsat and Envisat SAR images. IEEE Transactions on Geoscience and Remote Sensing, 45(3), pp. 746–755.

Song, J. H., Venkatesh, S. S., Conant, E. A., Arger, P. H., Sehgal, C. M., 2005. Comparative analysis of logistic regression and artificial neural network for computer-aided diagnosis of breast masses. Academic Radiology, 12(4), pp. 487–495.

Stathakis, D., Topouzeils, K. N., Karathanassi, V., 2006. Large-scale feature selection using evolved neural network. In: Proceedings of SPIE, Image and Signal Processing for Remote Sensing XII, edited by Bruzzone, L.,SPIE ETATS-UNIS, Bellingham Washington, p. 6365.

Topouzelis, K. N., 2008. Oil spill detection by SAR images: dark formation detection, feature extraction and classification algorithms. Sensors, 8(10), pp. 6642–6659.

UNOSAT, 2006. Satellite identification of major oil spill off the coast of Guimaras Island, Philippines. Retrieved from http://www.unitar.org/unosat/node/44/771.

Van Doorn, A. M., Bakker, M. M., 2007. The destination of arable land in a marginal agricultural landscape in South Portugal: an exploration of land use change determinants. Landscape Ecology, 22, pp. 1073-1087.